Available online at www.sciencedirect.com
SCIENCE DIRECT
Journal of Catalysis 241 (2006) 66–73
JOURNAL OF CATALYSIS
www.elsevier.com/locate/jcat

Reversibility of structural collapse in zeolite Y: Alkane cracking and characterization

Bin Xu [a], Franco Rotunno [b], Silvia Bordiga [b,*], Roel Prins [a], Jeroen A. van Bokhoven [a,*]

[a] *Institute for Chemical and Bioengineering, ETH Zurich, 8093 Zurich, Switzerland*
[b] *Centre of Excellence NIS – Dipartimento di Chimica I.F.M., Università di Torino, Via P. Giuria 7, I-10125 Torino, Italy*

Received 20 October 2005; revised 10 March 2006; accepted 17 April 2006

Available online 30 May 2006

Abstract

The structural collapse and the reconstruction of Brønsted acid sites in zeolite Y were investigated by combining propane monomolecular cracking with various structural characterization techniques. Destruction of Brønsted acid sites, together with a loss of catalytic activity, was found after calcination and exposure to moisture at room temperature. A loss in long-range structure was observed by XRD. Adsorption of NH_3 before exposure to air prevents the structural collapse of Brønsted acid sites and the loss of catalytic activity. The collapsed Brønsted acid sites and long-range order recover fully after thermal treatment with NH_3 at moderate temperature, as does the catalytic activity. Reheating of HY causes further structural collapse. Water molecules are involved in structural destruction, and also play a role in structural recovery with ammonia. The structure of zeolites is very sensitive to temperature and presence of moisture. Because various characterization methods are preceded by various pretreatment methods, the zeolite structure probed by these methods is not necessarily the same.

Keywords: Reversibility of structural collapse; Alkane cracking; Monomolecular cracking; Zeolite Y; Zeolite characterization; Acidity

1. Introduction

Because Brønsted acid sites are active in cracking, alkylation, and isomerization reactions [1,2], protonic zeolites are important catalysts in oil refining, petrochemistry, and fine chemical production. As new zeolite structures and new applications demonstrate, zeolites are a major area of scientific and industrial research [3–8]. Because of the susceptibility of the Al–O bonds to hydrolysis, acidic zeolites are unstable to heating in the presence of steam. The stability depends on the structure and the Si/Al ratio. Hydration leads to the removal of aluminum atoms from the framework to create non-framework aluminum and Lewis acid sites, whose structure and location are still being debated [9–11]. Mesopores often form during dealumination [12–18], and XRD reveals a loss of crystallinity [18]. For example, dealumination of zeolite Y in its own moisture or with the controlled addition of steam leads to ultra-stable zeolite Y (USY) [19,20], which is widely used in catalytic reactions, of which fluid catalytic cracking (FCC) is the most important.

Brønsted acid sites are directly related to tetrahedrally coordinated framework aluminum species, indicated by a peak in the ^{27}Al MAS NMR spectrum of a zeolite at about 60 ppm. In 1967, Kerr [21] reported that H-Y zeolite is unstable in the presence of water at room temperature. In zeolite Beta, octahedrally coordinated aluminum forms and can be converted to tetrahedral aluminum by adsorption of basic molecules, such as ammonia, as well as by substitution of the protons by sodium and potassium cations [22]. The presence of aluminum species that reversibly convert coordination on ammonia adsorption was also found in the zeolites ZSM-5 [10], MOR [23], and Y [24]. Similar behavior was observed in amorphous silica aluminas [23]. In acidic zeolites, the transformation of the coordination of aluminum from tetrahedral to octahedral occurs at room temperature after contact with moisture; at temperatures above 400 K, octahedral coordination is unstable [25,26] and reverts back to tetrahedral coordination, although the Brønsted acid site is not restored [23].

* Corresponding authors.
E-mail addresses: silvia.bordiga@unito.it (S. Bordiga), j.a.vanbokhoven@chem.ethz.ch (J.A. van Bokhoven).

0021-9517/$ – see front matter
doi:10.1016/j.jcat.2006.04.009

The change in aluminum coordination alters the number of Brønsted acid sites in the catalyst, which is directly related to the catalytic activity [27]. It has been reported that catalytic activity increases with the number of Brønsted acid sites in hexane cracking over zeolite Y [28,29] and ZSM5 [9,30], and in isobutene cracking over zeolite Y [31]. Steam activation is generally applied to activate zeolites [18,31,32]. Increased catalytic activity is generally explained by enhanced acidity of the remaining Brønsted acid sites [33,34]. Recently, enhanced participation of catalytically active sites by augmented adsorption of reactants has been proposed [35,36]. An important parameter in zeolite catalysts is the number of Brønsted acid sites that participate in the reaction. For example, it has been proposed that in zeolites Y and Beta, not all tetrahedral aluminum atoms contribute to strong Brønsted acid sites and activity [37]. Biaglow et al. showed that strong Brønsted acid sites in zeolite Y that decompose propyl amine molecules are associated with the high-frequency hydroxyl stretch vibration at 3640 cm^{-1} [38], which are the Brønsted acid sites pointing into the supercage.

In this study, the reversibility of structural changes of acidic zeolite Y was investigated by means of various characterization techniques and the structural changes were related to the catalytic activity of the zeolitic materials. The catalytic activity of the Brønsted acid sites was determined by monomolecular cracking of propane. When performed in the monomolecular reaction regime, the alkane is protonated by the zeolitic proton and, in the case of propane, cracked into methane and ethylene or dehydrogenated to propene and hydrogen:

$$C_3H_8 \xrightarrow{\text{cracking}} CH_4 + C_2H_4 \quad (1)$$

$$\xrightarrow{\text{dehydrogenation}} H_2 + C_3H_6. \quad (2)$$

Running the reaction at high temperature and low conversion prevents bimolecular reactions [39,40].

2. Experimental

2.1. Samples

NaY (LZ-Y54, UOP, Molecular Sieve Division, Si/Al = 2.6) was converted to NH_4Y by triple ion exchange at 353 K with 1 M NH_4NO_3. The residual Na content was determined by atomic absorption spectroscopy and was <0.05% of the aluminum content. Table 1 gives the treatments and nomenclature of the samples. To investigate the effect of moisture on the acid sites, about half of all the NH_4Y was calcined for 6 h at 823 K at a heating rate of 1 K/min and, after cooling to room temperature, exposed to air to form HY. To investigate the recovery of the original structure, several treatments were performed on the NH_4Y and HY samples. (NH_3)HY was obtained by calcination of NH_4Y at 823 K and switching to a flow of 10% NH_3 in He during the cooling of the sample from 423 K to room temperature [41,42]. Ammonia was adsorbed from a flow of 10% NH_3 in He on HY at 423 K to yield $H(NH_3)Y$. HY-723-423NH_3 was formed by heating HY to 723 K and switching to a flow of 10% NH_3 in He while cooling the sample from 423 K to room temperature. Calcination of HY at 723 K produced sample HY-723-RT. The influence of H_2O and temperature on this treatment was studied by infrared spectroscopy on HY. Adsorption of ammonia was carried out at room temperature following two procedures: (1) after activation at 723 K for 1 h, producing HY-723-RTNH_3, and (2) after activation at 723 K and subsequent room temperature adsorption of 2–2.7 kPa of H_2O, giving HY-723-RT$H_2O + NH_3$.

Table 1
Sample treatments and nomenclature

Sample	Starting material	Treatment	Exposed to air after treatment?
NH_4Y	–	–	–
HY	NH_4Y	Calcination at 823 K	Yes
(NH_3)HY	NH_4Y	Calcination at 823 K; cooled from 423 K to RT under NH_3	Yes
$H(NH_3)Y$	HY	Exposed to NH_3 at 423 K	Yes
HY-723-423NH_3	HY	Heated at 723 K in He; cooled from 423 K to RT under NH_3	Yes
HY-723-RT	HY	Heated at 723 K in He	Yes
HY-723-RTNH_3[a]	HY	Heated at 723 K in vacuum; RT exposure to NH_3	No
HY-723-RT$H_2O + NH_3$[a]	HY	Heated at 723 K in vacuum; RT exposed to H_2O and NH_3	No

[a] Treatments were performed in the IR apparatus.

2.2. Characterization

Nitrogen physisorption measurements were performed at liquid nitrogen temperature in a Micromeritics ASAP 2000 apparatus. Before the measurements, all of the samples were degassed at 723 or 423 K overnight. The surface area was determined by the BET method, and the micropore volume was determined from the intercept of the linear part of the *t*-plot. XRD patterns were obtained by spinning capillaries (0.3 mm diameter), filled with the samples, on a Siemens D-5000 powder X-ray diffractometer (Cu-K_α radiation) with Bragg–Brentano geometry. The aluminum content of the framework was determined using the established relationship between unit cell size and number of aluminum atoms in the unit cell [43,44]. MAS NMR spectra were measured at 104.287 MHz on a Bruker Advance AMX-400 spectrometer at a spinning rate of 12 kHz using a 4-mm probe head. Before the MAS NMR measurements, the samples were hydrated by placing them in an atmosphere saturated with moisture from a solution of 1 M NH_4NO_3. In ^{27}Al MAS NMR, a single pulse length of $\pi/6$ was used. In ^{29}Si MAS NMR, a high-power decoupling pulse sequence (HPDEC) and a relaxation delay of 6 s were used. The ^{29}Si chemical shifts were referenced to octakis-(trimethyl siloxy)silsesquioxane. For the FTIR measurements, self-supporting pellets (10–15 mg) were positioned in a laboratory-constructed heated cell equipped with KBr windows and connected to a glass vacuum line capable of attaining a residual vacuum of $<10^{-3}$ Pa. The spectra were recorded

at room temperature at 2 cm^{-1} resolution on a Bruker IFS28 FTIR spectrophotometer equipped with an MCT detector and a Globar MIR source. Before measurement, the samples were activated for 1 h in vacuum at 723 K with a heating ramp of 6 K/min. For selected samples, the number of Brønsted acid sites was determined using IR spectroscopy after pyridine adsorption. IR was performed in a flow cell on a Bio-Rad Excalibur FTS 3000 IR spectrometer. After activation at 773 K, the samples were treated for 10 min at 393 K in a He flow of 20 mL/min saturated at 273 K with pyridine, which has a vapor pressure of 550 Pa. IR spectra were recorded after flowing He for 1 h at 423 K and for 1 h at 623 K. The numbers of Brønsted acid sites were determined using the integrated molar extinction coefficients for the infrared absorption band of pyridinium of 1.67 cm/μmol, mode 19b at 1545 cm^{-1} [45].

2.3. Propane monomolecular cracking

The catalytic reaction was performed in a setup with six parallel-flow, tubular quartz reactors, with 10% propane in argon (10 kPa partial pressure for propane) between 675 and 875 K and 100 kPa total pressure. The Arrhenius plots were determined in this temperature range. During the measurements, the temperature was varied in a random manner, and it was confirmed that this did not affect the outcome. The rates of reaction measured at 823 K are reported. The flow rates varied from 5 to 50 mL/min; the catalyst weights from 50 to 200 mg. Before the reaction, the catalysts were activated in a reactor in 10% oxygen in argon at 878 K for 1 h with a heating ramp of 2 K/min. The products were analyzed in the effluent gas stream with an on-line Agilent 3000 MicroGC gas chromatograph. The MicroGC comprises three self-contained GC modules, each consisting of an injector, column, flow control valves, and a thermal conductivity detector, which can be used to analyze hydrogen, natural gas, and refinery gases. Three columns were used: MolSieve 5A, PLOT U, and Alumina PLOT.

The reaction rate was calculated as [40]:

$$r_i = \frac{X_i V}{m_{\text{cat}}}, \tag{3}$$

where X_i is the individual reaction conversion, V is the volumetric flow rate of the feed, and m_{cat} is the weight of the catalyst. The apparent activation energy and pre-exponential term are defined as

$$\ln r = \frac{-E_{\text{app}}}{RT} + \ln A_{\text{app}}. \tag{4}$$

The apparent activation energies were determined from the slope of the Arrhenius plot. The reaction conditions were chosen so that the molar ratios of C_1 and $C_2^=$, as well as of H_2 and $C_3^=$, were unity and no hydrocarbons with more than three atoms were detected. Conversion was kept below 10%. We discuss the conversion to the cracking products methane and ethene here.

3. Results

3.1. Reaction kinetics

Table 2 lists the reaction rates at 823 K, the apparent activation energies, and the selectivity to cracking of all of the samples. At 823 K, the reaction rates of cracking of the parent sample NH_4Y and of $(NH_3)HY$ are the same, whereas the reaction rate of $H(NH_3)Y$ is slightly lower. The rate of HY is much lower than the rates of NH_4Y, $(NH_3)HY$, and $H(NH_3)Y$. The reaction rate of HY-723-423NH_3 is slightly higher than that of HY.

Fig. 1 shows the Arrhenius plots of the monomolecular cracking of propane of the three samples NH_4Y, $H(NH_3)Y$, and HY. The apparent activation energies of NH_4Y and $H(NH_3)Y$ are 165 and 168 kJ/mol (Table 2), respectively, obtained by averaging three measurements on newly prepared samples. These values are within the uncertainty of the measurement (±5 kJ/mol). The value for $(NH_3)HY$ is very similar, 162 kJ/mol. The apparent activation energies of the samples HY and HY-723-423NH_3 are much higher, 208 and 269 kJ/mol, respectively. The cracking selectivity also differs for NH_4Y, $(NH_3)HY$, and $H(NH_3)Y$ and for HY and HY-723-423NH_3. The former samples have a higher selectivity to cracking, and the latter have a higher selectivity to dehydrogenation.

Table 2
Reaction rates and activation energies of monomolecular cracking of propane over treated zeolite samples

Sample	Rate-cracking[a] $\times 10^{-6}$ (/(g s bar))	Activation energy (kJ/mol)	100 × cr/(cr+de)[b]
NH_4Y	0.29	165	60
HY	0.05	208	38
$(NH_3)HY$	0.30	168	70
$H(NH_3)Y$	0.21	162	57
HY-723-423NH_3	0.08	269	42

[a] At 823 K.
[b] Selectivity to cracking (in %).

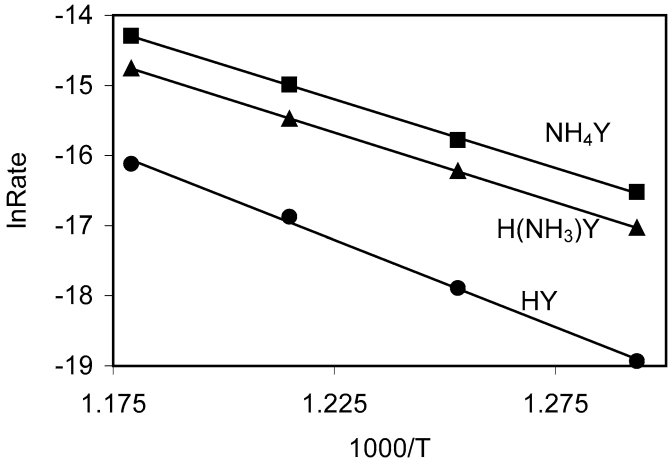

Fig. 1. Arrhenius plots of monomolecular cracking of propane over NH_4Y(■), HY(●), and $H(NH_3)Y$(▲).

Table 3
Characteristics of the samples[a]

Sample	Si/Al AAS	Si/Al ^{29}Si MAS NMR	%Td Al ^{27}Al MAS NMR[b]	Unit cell a_0 (Å)	Surface area (m^2/g)	Micropore volume (cm^3/g)	Brønsted acid sites[c] (mmol/g)	Brønsted acid sites[d] (mmol/g)
NH_4Y	2.6 (53)	2.4 (56)	100 (53)	24.720 (52)	810	0.32	1.1	0.6
HY	2.6	2.6 (53)	93 (49)	24.643 (43)	450	0.18	0.2	0.07
$(NH_3)HY$	2.6	n.d.	100 (53)	24.705 (50)	770	0.31	n.d.	n.d.
$H(NH_3)Y$	2.6	n.d.	100 (53)	24.705 (50)	770	0.31	0.8	0.4
HY-723-423NH_3	2.6	n.d.	–	24.580 (36)	230	0.09	n.d.	n.d.
HY-723-RT	2.6	3.4 (44)	–	24.580 (36)	n.d.	n.d.	n.d.	n.d.

n.d., Not determined.
[a] The corresponding numbers of aluminum per unit cell are given in brackets.
[b] Only the narrow peak at about 60 ppm is considered.
[c] Pyridine IR after desorption at 423 K.
[d] Pyridine IR after desorption at 623 K.

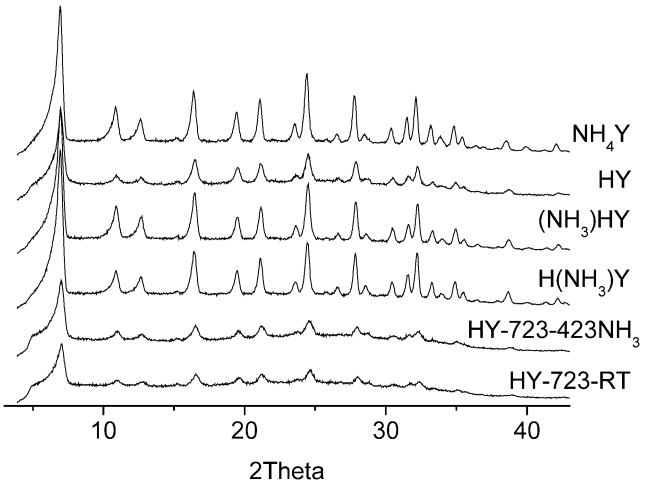

Fig. 2. XRD patterns of NH_4Y and the treated samples.

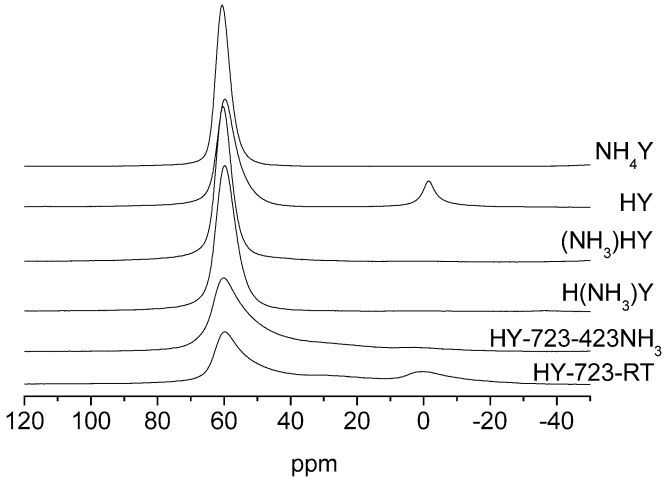

Fig. 3. ^{27}Al MAS NMR of NH_4Y and the treated samples.

3.2. Characterization

The BET surface areas and micropore volumes after degassing at 723 K are given in Table 3 (columns 6 and 7). NH_4Y had the highest surface area (810 m^2/g). $(NH_3)HY$ and $H(NH_3)Y$ had identical values (770 m^2/g). The micropore volumes were also very similar (0.32, 0.31, and 0.31 cm^3/g, respectively). HY had a much lower surface area (450 m^2/g) and micropore volume (0.18 cm^3/g). Degassing HY at 423 K yielded essentially the same values. HY-723-423NH_3 had the lowest surface area (230 m^2/g) and micropore volume (0.09 cm^3/g), less than half the values of the parent sample NH_4Y. The number of Brønsted acid sites, determined with IR after the adsorption of pyridine and desorption at 423 and 623 K, shows that NH_4Y and $H(NH_3)Y$ had a high concentration of Brønsted acid sites and that the amount depended on the temperature of pyridine desorption. HY contained <20% of the amount of Brønsted acid sites in NH_4Y.

Fig. 2 shows the XRD patterns of NH_4Y and the treated samples. The samples were not pretreated before measurement. NH_4Y, $(NH_3)HY$, and $H(NH_3)Y$ showed similar patterns and high crystallinity. The patterns of HY, HY-723-423NH_3, and HY-723-RT showed less-intense and broader diffraction peaks, indicating a loss of crystallinity, especially for the latter two. In HY, the loss of crystallinity is likely due to increased disorder and loss of long-range order because of the formation of local defect sites and partial dealumination of the structure (vide infra). The unit cell parameters are given in Table 3. The corresponding number of aluminum atoms per unit cell was with 43 significantly lower in HY than in NH_4Y, $(NH_3)HY$, and $H(NH_3)Y$, where it was about 50. Heating HY and exposure to air resulted in a further decrease in the aluminum content of the framework; samples HY-723-423NH_3 and HY-723-RT had 36 aluminum atoms per unit cell.

Fig. 3 shows the ^{27}Al MAS NMR spectra of NH_4Y and the treated samples. The samples were stored in a controlled wet environment before measurement. For NH_4Y, $(NH_3)HY$, and $H(NH_3)Y$, a single peak at 60 ppm was observed, assigned to tetrahedrally coordinated framework aluminum. The width of the peak in the spectrum of $H(NH_3)Y$ was larger than that of the other two samples. The spectrum of HY showed two peaks, one at 60 ppm, attributed to tetrahedrally coordinated aluminum, and the other at 0 ppm, assigned to octahedrally coordinated aluminum. The peak for tetrahedrally coordinated aluminum was slightly broadened, showing disorder in the structure. HY-723-423NH_3 had a broad tetrahedral peak and a small fraction of octahedrally coordinated aluminum. Moreover, a low-intensity signal at 20–40 ppm was detected and was attributed

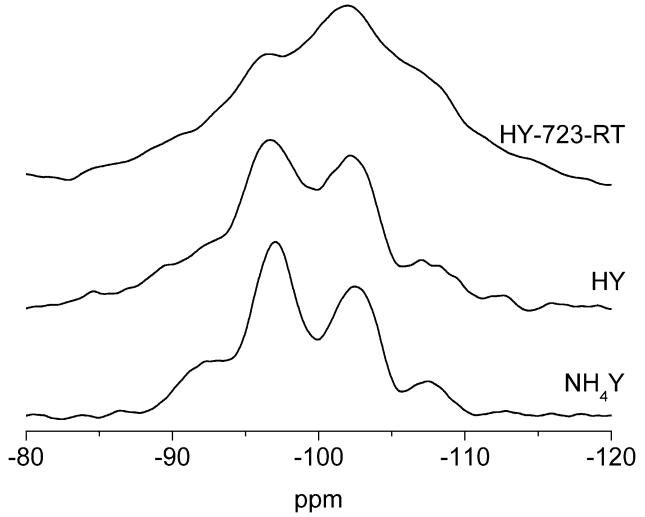

Fig. 4. ^{29}Si MAS NMR spectra of NH_4Y, HY, and HY-723-RT.

to penta-coordinated aluminum or distorted tetrahedrally coordinated aluminum [46]. HY-723-RT showed enhanced intensity of octahedrally coordinated and penta-coordinated or distorted tetrahedrally coordinated aluminum. Assuming that the sharp tetrahedrally coordinated aluminum peak in the spectra of NH_4Y, HY, $(NH_3)HY$, and $H(NH_3)Y$ correlates to framework aluminum, 49 aluminums per unit cell are estimated for HY and 53 aluminums per cell are estimated for NH_4Y, $(NH_3)HY$, and $H(NH_3)Y$.

From ^{29}Si MAS NMR data [47], the Si/Al ratios of all silica-alumina phases in the samples can be estimated. These phases are the crystalline zeolite and any amorphous silica-aluminas that may have been formed during the treatments. For selected samples, ^{29}Si MAS NMR data are presented in Fig. 4. Analysis of the spectrum of NH_4Y gave a Si/Al ratio of 2.4 (Table 3), which is close to the bulk value as determined from atomic absorption spectroscopy. The spectrum of HY showed a decreased intensity of the peak at about 97 ppm, which is ascribed to a silicon atom with two aluminum next-nearest neighbors [Q^4(2Al)]. A corresponding increase in the Si/Al ratio to 2.6 of the silica-alumina phases was observed, which correlates with a decrease of $<10\%$ of the framework aluminum content, in reasonable agreement with an octahedrally coordinated aluminum content of 7%. The spectrum of HY-723-RT showed broadened peaks and increased intensity at the more negative ppm values, indicative of significant dealumination, which is also demonstrated by the higher Si/Al ratio of 3.4.

The IR spectra of NH_4Y, HY, $H(NH_3)Y$, and HY-723-$423NH_3$, measured at room temperature after vacuum activation at 723 K (Fig. 5), showed that ammonia was completely removed and the samples were in protonic form. To compare the intensities of the OH peaks of the different samples, all of the spectra were normalized in intensity by giving the overtones and combination modes of the zeolitic framework at about 1700–2000 cm^{-1} equal intensity. The parent sample, NH_4Y, exhibited bands at 3640 and 3545 cm^{-1}, assigned to Brønsted acid sites in the super cages (high frequency [HF]) and Brønsted acid sites in the sodalite cages (low frequency [LF]),

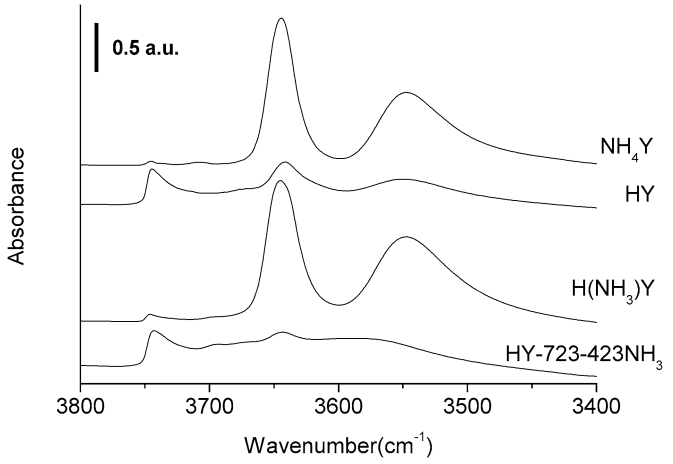

Fig. 5. FTIR spectra of NH_4Y and the treated samples in the region of OH stretching vibration.

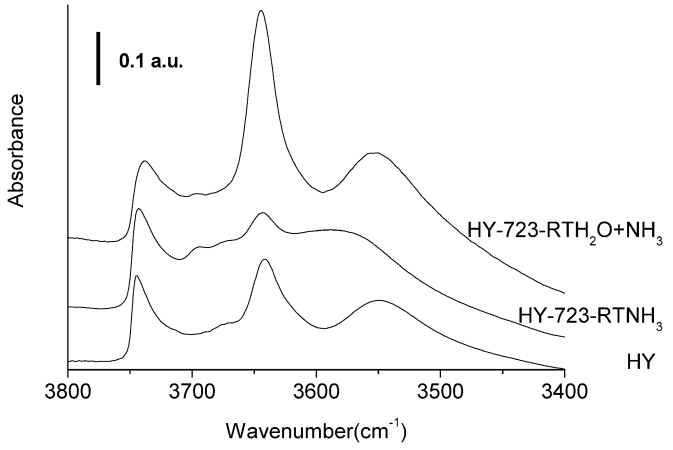

Fig. 6. FTIR spectra of HY and its treated samples in the region of OH stretching vibration.

respectively [48]. The band at 3745 cm^{-1} is assigned to the silanol OH vibration. The IR spectrum of $H(NH_3)Y$ was almost identical to that of NH_4Y. The spectrum of HY showed a much lower intensity of the HF and LF bands and a higher intensity of the silanol band at 3745 cm^{-1}. Compared to HY, the spectrum of HY-723-$423NH_3$ showed even weaker HF and LF bands. Fig. 6 shows the infrared spectra of HY and of the in situ treated samples recorded at room temperature after reactivation and ammonia removal at 723 K. The number of Brønsted acid sites in these samples decreased in the order HY-723-$RTH_2O + NH_3$ > HY > HY-723-$RTNH_3$, which indicates that Brønsted acid sites are restored only when small amounts of H_2O are present.

4. Discussion

4.1. Catalytic activity

The propane-cracking activities and apparent activation energies of samples NH_4Y, $(NH_3)HY$, and $H(NH_3)Y$ are very similar. In contrast, the calcined sample, which was exposed to air at room temperature (HY), showed a much lower cracking

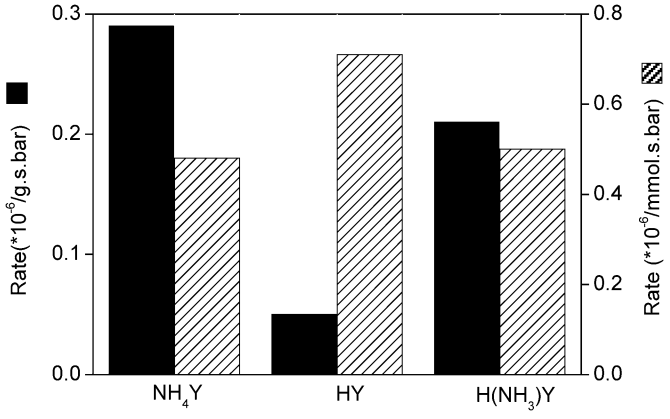

Fig. 7. Catalytic activity per gram (solid bars) and normalized per H^+ site, as determined by IR after pyridine adsorption (dashed bars); see text for details.

activity per gram and a higher apparent activation energy, indicating that the structure and number of the catalytically active sites had changed. Fig. 7 compares the catalytic activities per gram of NH_4Y, HY, and $H(NH_3)Y$ with the catalytic activities normalized by the number of Brønsted acid sites, as determined by IR after pyridine adsorption and desorption at 623 K. The activities per Brønsted acid site for NH_4Y and $H(NH_3)Y$ are the same and slightly lower than the activity for HY. The activity per site and the number of sites in NH_4Y and $H(NH_3)Y$ are very similar. The activity per site in HY differs, which was also indicated by its different activation energy (Table 2).

All of the characterization methods indicate that HY is partially dealuminated and has low crystallinity and surface area and a decreased number of Brønsted acid sites. Its structure is a function of temperature (vide infra). Structural collapse occurs at room temperature after exposure to moisture, as was previously demonstrated by in situ Al XAS, which showed the formation of octahedrally coordinated aluminum at room temperature after exposure of an acidic Y zeolite to moisture [25]. Heating this zeolite causes further structural damage, as shown by the loss of crystallinity and intensity in the stretching OH region in the IR spectra (Fig. 5). The catalytic measurements were performed at high temperature, so characterization after additional heat treatment is most representative of the structures under catalytic reaction conditions.

$H(NH_3)Y$ was made from HY by adsorption of gaseous ammonia at 423 K; its very similar kinetic parameters to those of the parent sample NH_4Y demonstrate that treatment with NH_3 results in virtually full recovery of HY's catalytic activity. The characterization results of these samples are also very similar. The catalytic behavior of sample $(NH_3)HY$, which was made by calcining the parent sample NH_4Y and exposing it to NH_3 before exposure to air, confirms that the NH_3 treatment maintained the catalytic activity of the parent sample NH_4Y after calcination, as was proposed previously [41,42,49,50].

In summary, the catalytic cracking of propane over zeolite Y and the treated samples shows that the activity does not change when the material in its acidic form is not exposed to air. An inactive catalyst can be recovered by NH_3 treatment at 423 K; however, if this catalyst is heated first, then recovery will be incomplete.

4.2. *Reversibility of the structure of Brønsted acid sites of zeolite catalysts*

Based on the spectroscopic results and according to previous proposals [22–24], Scheme 1 presents the structures of the Brønsted acid sites in every state (NH_4Y, HY, and the ammonium-treated HY). Species (a) represents the structure of the catalytically active site in the ammonium form of the zeolite. The aluminum is tetrahedrally coordinated. Species (b) contains the bridging hydroxyl group of a Brønsted acid site formed after NH_3 removal. In this state, the OH vibration of the Brønsted acid sites was detected by IR (Fig. 5) and tetrahedrally coordinated aluminum detected by Al *K*-edge XAS measurements [51]. This sample is catalytically active. After calcination and exposure to moisture in air at room temperature, some of the Brønsted acid sites were converted into species (c), identified by octahedrally coordinated aluminum in the ^{27}Al MAS NMR (Fig. 3) and Al *K*-edge XAS [51]. The exact structure of the octahedrally coordinated aluminum remains unknown; however, the peak in the ^{27}Al MAS NMR spectrum is very sharp (500 Hz), strongly suggesting that either a symmetric species or a very mobile species forms that is highly dehydroxylated, almost ion-like, and strongly hydrated. Theoretical calculations suggest that the dehydroxylation of aluminum in the framework can occur and that an extra-framework species

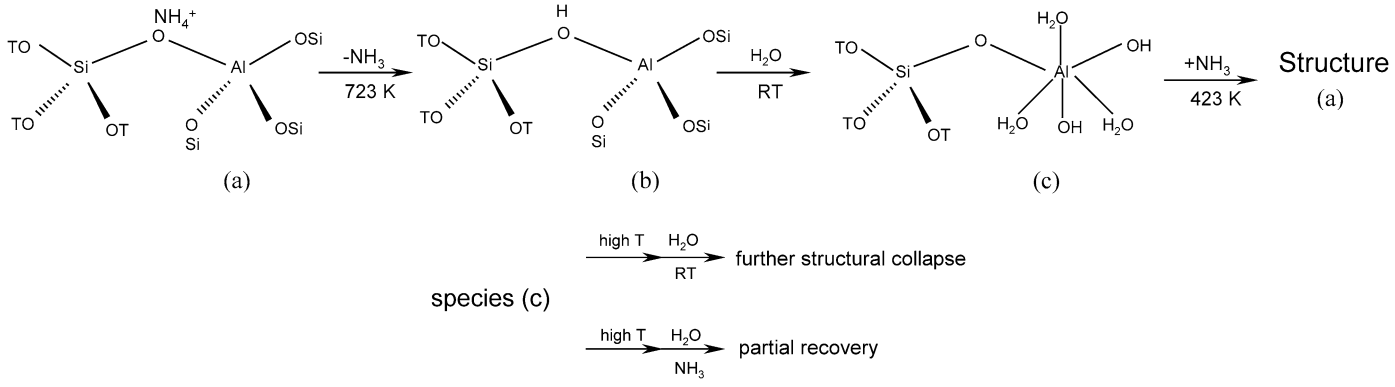

Scheme 1. Structure of Brønsted acid sites during activation and deactivation of NH_4Y (a) NH_4Y; (b) [HY] formed after ammonia removed from NH_4Y; (c) change of the aluminum coordination from tetrahedral to octahedral by room temperature exposure of calcined NH_4Y to air [23].

forms that is coordinated to its original position by a network of hydrogen bonds [52]. The presence of octahedrally coordinated aluminum correlates with the results of Si MAS NMR and XRD indicating a higher Si/Al ratio in this sample. Comparing the numbers of Brønsted acid sites in the parent sample NH_4Y and HY, determined in the hydroxyl region in the IR spectra and the py-H^+ region after pyridine adsorption, indicates that few Brønsted acid sites remain in HY and that a large number of silanol groups are formed (Fig. 5; Table 3). These few Brønsted sites explain the strongly decreased catalytic activity of this sample. A similar phenomenon has been observed on NH_4-beta and H-beta zeolites [49].

The structural collapse of zeolite HY can be reverted by ammonia treatment at temperatures below 423 K, resulting in species (a) [22–24,53,54], as indicated by tetrahedral aluminum in ^{27}Al MAS NMR and Al *K*-edge XAS [51], the high intensity of the Brønsted acid sites in IR, high crystallinity, recovered unit cell parameters, and microporous volume with XRD and nitrogen physisorption. However, treating HY at high temperature causes further structural damage, even more so when exposed to air afterward, which can no longer be fully repaired by ammonia (Scheme 1). ^{27}Al and ^{29}Si MAS NMR, IR, and XRD all showed further structural damage after re-exposure to air of the high-temperature-activated zeolite HY.

In HY exposed to air, a significant fraction of the Al–O and Si–O bonds are hydrolyzed and broken, leading to a partially amorphous structure and a considerable loss of long-range order and micropore volume. However, large parts of the network of the Si–O–T bonds remain intact, enabling full recovery of the structure.

This and previous reports [21–24,53,54] have shown that moisture partially destroys an acidic zeolite; with a base like ammonia and pyridine, the collapsed structure fully recovers. Our IR measurements indicate that H_2O also plays a role in structural recovery. If HY is heated to 723 K and completely dehydrated, then adsorption of gaseous ammonia at 393 K does not result in reconstruction of the Brønsted acid sites (HY-723-RTNH_3; Fig. 6), and the structure collapses further (Scheme 1). Partial reconstruction of the Brønsted acid sites occurs only after a small amount of H_2O is added (Fig. 6; Scheme 1). H_2O may enable atom mobility through formation of hydroxyl groups on the zeolite surface, thus enabling reconstruction with NH_3. Hydroxylation reactions are base-catalyzed, and thus the role of NH_3 is to catalyze this reaction. Moreover, NH_4OH may form, which aids formation of the Brønsted acid sites and produces NH_4^+ ions, which charge-compensate the zeolite framework. Reversible structural changes are a general property of zeolites [10,22,26] and amorphous silica-aluminas [23,55]. The amount of octahedrally coordinated aluminum is a function of structure type [10,22–24] and of the Si/Al ratio of the framework [56]. Different structure types have different T-connectivities, aluminum proximities, and pore sizes, which affect the stability of the structure. Zeolites with a high framework Si/Al ratio are very hydrophobic, which may protect the zeolite framework from attack by water molecules. The low Si/Al ratio, and thus the high aluminum content of zeolite NH_4Y, make this zeolite particularly unstable and sensitive to moisture. The high proton density leads to partial dealumination already at room temperature after exposure to moisture from the air.

4.3. Different characterization techniques reveal different states of zeolite catalysts

Spectroscopic measurements are preceded by sample pretreatment, which often differs for each characterization technique. Because the structures of zeolites are sensitive to their environment, they alter during the pretreatment of the characterization methods. ^{27}Al MAS NMR is generally used to study the hydrated state of catalysts. The dehydrated state of catalysts is studied by such techniques as nitrogen physisorption, FTIR, ^{1}H MAS NMR, and kinetic measurements, all of which are performed after catalyst activation at high temperature. Because different techniques reveal different zeolite structures, direct comparison of the results of various techniques is often difficult. True in situ methods are essential to determine the zeolite structure under catalytically relevant conditions. Several techniques, including X-ray absorption spectroscopy, XRD, and, to some extent, NMR, can determine the zeolite structure under well-defined conditions, aiding the direct comparison of results of other characterization techniques and identifying structure–performance relationships.

5. Conclusion

This paper has described the conditions that induce the destruction and reconstruction of zeolitic Brønsted acid sites. Some of the Brønsted acid sites in the acidic form of the zeolites collapse after contact with moisture from the air. Heating this partially dealuminated zeolite causes further structural collapse and a loss of catalytic activity at high temperature. However, treatment of the collapsed Brønsted acid sites with NH_3 results in recovery of the catalytic activity. The presence of H_2O molecules aids in structural recovery. Different characterization methods reveal different zeolite structures, because of the structural changes occurring during sample preparation.

Acknowledgments

The authors thank Anuji Abraham for her help with the MAS NMR measurements.

References

[1] J. Ward, J. Catal. 11 (1968) 259.
[2] J. Abott, F.N. Guerzoni, Appl. Catal. 85 (1992) 173.
[3] A. Corma, M. Diaz-Cabanas, J. Martinez-Triguero, F. Rey, J. Rius, Nature 418 (2002) 514.
[4] A. Corma, L.T. Nemeth, M. Renz, S. Valencia, Nature 412 (2001) 423.
[5] A. Corma, V. Fornes, S.B. Pergher, T.L.M. Maesen, J.G. Buglass, Nature 396 (1998) 353.
[6] X.H. Bin, P.Y. Feng, G.D. Stucky, Science 278 (1997) 2080.
[7] S.M. Kuznicki, V.A. Bell, S. Nair, H.W. Hillhouse, R.M. Jacubinas, C.M. Braunbarth, B.H. Toby, M. Tsapatsis, Nature 412 (2001) 720.
[8] M.E. Davis, Nature 417 (2002) 813.
[9] W.O. Haag, R.M. Lago, P.B. Weiss, Nature 309 (1984) 589.

[10] G.L. Woolery, G.H. Kuehl, H.C. Timken, A.W. Chester, J.C. Vartuli, Zeolites 19 (1997) 288.
[11] P.V. Shertukde, W.K. Hall, J.M. Dereppe, G. Marcelin, J. Catal. 139 (1993) 468.
[12] R. Dutatre, L.C. de Menorval, F. Di Renzo, D. McQueen, F. Fajula, P. Schulz, Microporous Mater. 6 (1996) 311.
[13] D. Vergani, R. Prins, H.W. Kouwenhoven, Appl. Catal. A. 163 (1997) 71.
[14] C.A. Henriques, J.L. Monteiro, P. Magnoux, M. Guisnet, J. Catal. 172 (1997) 436.
[15] K.H. Lee, Y.W. Lee, B.H. Ha, J. Catal. 178 (1998) 328.
[16] K.H. Lee, B.H. Ha, Microporous Mesoporous Mater. 23 (1998) 211.
[17] R. Giudici, H.W. Kouwenhoven, R. Prins, Appl. Catal A. 203 (2000) 101.
[18] R.A. Beyerlein, C. Choi-Feng, J.B. Hall, B.J. Huggins, G.J. Ray, Top. Catal. 4 (1999) 91.
[19] Q.L. Wang, G. Giannetto, M. Torrealba, G. Pérot, C. Kappenstein, M. Guisnet, J. Catal. 130 (1991) 459.
[20] C.V. McDaniel, P.K. Maher, US Patents 3,292,192 (1966); 3,449,070 (1969).
[21] G.T. Kerr, J. Catal. 15 (1969) 200.
[22] E. Bourgeat-Lami, P. Massiani, F. Di Renzo, P. Espiau, F. Fajula, Appl. Catal. 72 (1991) 139.
[23] A. Omegna, J.A. van Bokhoven, R. Prins, J. Phys. Chem. B. 107 (2003) 8854.
[24] B.H. Wouters, T.-H. Chem, P.J. Grobet, J. Am. Chem. Soc. 120 (1998) 11419.
[25] J.A. van Bokhoven, A.M.J. van der Eerden, D.C. Koningsberger, Stud. Surf. Sci. Catal. 142 (2002) 1885.
[26] J.A. van Bokhoven, A.M.J. van der Eerden, D.C. Koningsberger, J. Am. Chem. Soc. 125 (2003) 7435.
[27] N. Katada, T. Kanai, M. Niwa, Microporous Mesoporous Mater. 75 (2004) 61.
[28] P.O. Fritz, J.H. Lunsford, J. Catal. 118 (1989) 85.
[29] F. Lonyi, J.H. Lunsford, J. Catal. 136 (1992) 566.
[30] D.H. Olson, W.O. Haag, R.M. Lago, J. Catal. 61 (1980) 390.
[31] R.A. Beyerlein, G.B. McVicker, L.N. Yacullo, J.J. Ziemiak, J. Phys. Chem. 92 (1988) 1967.
[32] F. Lonyi, J.H. Lunsford, J. Catal. 136 (1992) 566.
[33] C. Miradatos, D. Barthomeuf, J. Chem. Soc., Chem. Commun. 2 (1981) 39.
[34] R. Carvajal, P.J. Chu, J.H. Lunsford, J. Catal. 125 (1990) 123.
[35] J.A. van Bokhoven, B.A. Williams, W. Ji, D.C. Koningsberger, H.H. Kung, J.T. Miller, J. Catal. 224 (2004) 50.
[36] C.E. Ramachandran, B.A. Williams, J.A. van Bokhoven, J.T. Miller, J. Catal. 233 (2005) 100.
[37] S. Kotrel, M.P. Rosynek, J.H. Lunsford, J. Catal. 182 (1999) 278.
[38] A.I. Biaglow, D.J. Parrillo, R.J. Gorte, J. Catal. 144 (1993) 193.
[39] W.O. Haag, R.M. Dessau, R.M. Lago, Stud. Surf. Sci. Catal. 60 (1991) 255.
[40] T.F. Narbeshuber, H. Vinek, J.A. Lercher, J. Catal. 157 (1995) 388.
[41] P.J. Kunkeler, B.J. Zuurdeeg, J.C. van der Waal, J.A. van Bokhoven, D.C. Koningsberger, H. van Bekkum, J. Catal. 180 (1998) 234.
[42] G.H. Kuehl, US Patent 4,661,467 (1987).
[43] D.W. Breck, E.M. Flanigen, Molecular Sieves, Society of Chemical Industry, London, UK, 1968, p. 47.
[44] J.R. Sohn, S.J. Decanio, J.H. Lunsford, D.J. O'Donnell, Zeolites 6 (1986) 225.
[45] C.A. Emeis, J. Catal. 141 (1993) 347.
[46] J.A. van Bokhoven, A.L. Roest, D.C. Koningsberger, J.T. Miller, G.H. Nachtegaal, A.P.M. Kentgens, J. Phys. Chem. B. 104 (2000) 6743.
[47] G. Engelhardt, D. Michel, High Resolution Solid State NMR of Silicates and Zeolites, Wiley, Chichester, 1987, p. 211.
[48] F. Eder, M. Stockenhuber, J.A. Lercher, J. Phys. Chem. B. 101 (1997) 5414.
[49] L. Capek, J. Dedecek, B. Wichterlova, J. Catal. 227 (2004) 352.
[50] S. Altwasser, J. Jiao, S. Steuernagel, J. Weitkamp, M. Hunger, Stud. Surf. Sci. Catal. 154 (2004) 3098.
[51] J.A. van Bokhoven, Phys. Scr. T 115 (2005) 76.
[52] C. Busco, PhD Thesis, University of Torino, Italy (2003).
[53] J.A. van Bokhoven, D.C. Koningsberger, P. Kunkeler, H. van Bekkum, J. Catal. 211 (2002) 540.
[54] J.A. van Bokhoven, D.C. Koningsberger, P. Kunkeler, H. van Bekkum, A.P.M. Kentgens, J. Am. Chem. Soc. 122 (2000) 12842.
[55] S. Hitz, R. Prins, J. Catal. 168 (1997) 194.
[56] A. Abraham, S.H. Lee, C.H. Shin, S.B. Hong, R. Prins, J.A. van Bokhoven, Phys. Chem. Chem. Phys. 6 (2004) 3031.